Plasmonic metal decorated titanium dioxide thin films for enhanced photodegradation of organic contaminants

Pardon Nyamukamba, Lilian Tichagwa, Jane Catherine Ngila and Leslie Petrik

Abstract

Photocatalysis using titanium dioxide as photocatalyst is an efficient way for the removal of organic contaminants in water using solar energy. In this study, thin films of copper and silver were deposited on fused silica using the thermal evaporation technique. A 100 nm film of titanium dioxide (TiO_2) was then deposited on the plasmonic metal films using a sputter coating technique. The opposite order of deposition of the film was also explored. The prepared thin films were fully characterized using high resolution scanning electron microscopy (HRSEM), X-ray diffraction (XRD), atomic force microscopy (AFM) and Rutherford backscattering spectrometry (RBS). The effect of plasmonic metal film thickness, order of deposition and the use of bimetallic layers on the photocatalytic activity of the TiO_2 photocatalyst was evaluated using methyl orange as a model pollutant. It was shown that, the increase in Ag film thickness underneath the TiO_2 film increased the photocatalytic activity of the TiO_2 photocatalyst until an optimum film thickness of 20 nm was attained. In the case of copper, the increase in film thickness above 5 nm led to reduced photocatalytic activity. Silver was found to be a better plasmonic metal than copper in enhancing the photocatalytic activity of TiO_2 under UV light illumination. Cu was found to perform better when deposited underneath the TiO_2 film whereas Ag performed better when deposited on top of the TiO_2 photocatalyst film. The use of bimetallic layers was found to enhance TiO_2 photocatalytic activity more than monometallic layers.

1. Introduction

Access to adequate and safe drinking water is vital for human health hence it will remain a high priority. Due to an increase in population sizes and industrialization, the pressure on the available water resources for safe drinking water has increased. Many contaminants such as toxic metals, persistent organic contaminants from pharmaceutical industries, endocrine disruptors and dyes from textile industries are discharged into

the environment resulting in contamination of the available water resources. Among the various methods available for water purification, some conventional methods such as flocculation and coagulation, ultrafiltration and adsorption using activated carbon have the disadvantage of creating secondary pollution which requires further treatment, disposal of the solid waste and difficult regeneration of the adsorbent which makes these expensive options [1,2]. Besides the high operational costs, these methods could generate toxic secondary pollutants which can further pollute the environment [3].

These factors have led to the rapid development of alternative treatment methods to replace conventional methods, such as advanced oxidation processes (AOPs) which are very promising methods for treating contaminated water. Much attention has been given to photocatalysis due to its potential to degrade a wide range of recalcitrant organic contaminants into less harmful products at ambient temperature [4–6].

The TiO_2 photocatalyst only absorbs UV light which is a major drawback in its application. Several ways have been used to extend its absorption into the visible region which makes about 50% of the total solar radiation available and these include noble metal loading (plasmonic elements), ion doping, anion doping, dye sensitization and the use of composite semiconductors. The introduction of metallic nanostructures such as gold and silver into a semiconductor film to enhance photocatalytic activity by strong plasmonic effects has received attention recently [7]. The plasmonic elements increase the light absorption to boost the excitation of electrons in TiO_2 resulting in increased photoelectric conversion efficiency. Irradiating Au nanoparticles at their plasmon resonance frequency for instance, results in the creation of intense electric fields which increase the rate of electron-hole pair generation in semiconductors. This extends the photocatalytic activity of wide band gap semiconductors into the visible region of solar radiation. Previous studies have shown that the deposition of noble metals also reduces the recombination of the photo-generated electron−hole pairs resulting in enhanced photocatalytic activity [8–10].

Previously, TiO_2 photocatalysts were mainly used as a suspension in the form of a powder but the recovery of the photocatalyst adds unnecessary costs such as the filtration to purify the water. This prompted the coating of the photocatalyst on various surfaces which include silica, zeolite, activated carbon and quartz. Therefore in this study, the nanoparticles were deposited as thin films on fused silica which is transparent to light.

2

2. Experimental procedures

2.1 Materials

Hydrogen peroxide was purchased from Sigma Alddrich, sulphuric acid and bisphenol A were purchased from MET-U-ED, 3-mercaptopropyltrimethoxysilane from Alfa Aesar, hydrofluoric acid and 2-propanol were supplied by Associated Chemical Enterprises (Pty)(Ltd) and methyl orange was obtained from Merck. All reagents and solvents were used as received without further purification.

2.2 Silver and copper film deposition

Thin films of copper and silver were deposited on 3-mercaptopropyltrimethoxysilane (MPTMS) surface modified fused silica with dimensions of 2.5 cm by 3.5 cm, using the thermal evaporation technique. The method for the treatment of fused silica with MPTMS was reported in literature [11]. For the deposition of copper, the copper source material was loaded onto a tungsten sample holder and placed in the centre of the thermal evaporator's dome. A desired vacuum was created using a vacuum pump. The current was then increased slowly until the copper source material started to melt and evaporate. The evaporated material was deposited on fused silica support that was placed above the copper source. This system was fitted with an acoustic crystal monitor for controlling the amount of metal deposited. When the desired thickness was achieved, the swing arm shield was closed to prevent more material from depositing onto the fused silica supports followed by switching off the vacuum pump and allowing air into the chamber to release the vacuum. The same procedure was repeated for the deposition of silver. Table 1 shows the parameters used for the deposition of the metal thin films on the MPTMS treated fused silica.

Different thicknesses of the plasmonic elements were prepared and QPod.exe software was used for the film thickness determination. Bimetallic films were also prepared using the same procedure. The metal films were deposited one at a time, layer by layer. The sample description and codes of the prepared samples are given in Table 2.

Table 1
Experimental conditions used to prepare Cu and Ag thin films.

Parameter	Copper	Silver
Vacuum Pressure (Pascal)	3.0×10^{-3}	3.2×10^{-3}
Current (Amps)	95	100
Rate of deposition (nm/s)	*Variable (0–1.2)*	*Variable (0–1.2)*
Frequency (Hz)	591365.25	591365.25

3

2.3 TiO2 thin film preparation

TiO2 was deposited on top or below of the noble metal films using the electron sputter coating technique. In a typical experiment, the titanium source material and fused silica support to be coated were placed in the chamber of the sputter coating instrument. A vacuum was created and oxygen gas was introduced into the chamber to react with titanium to form the desired product (TiO2). The voltage used was between 460 and 465 V and the deposition rate of the TiO2 film was approximately 1 nm per minute. In order to obtain a 100 nm TiO2 film, the deposition was done for about 1 h 40 min. The parameters used for depositing the thin film of TiO2 were: current 0.28 amps, power 129 W, voltage 460−465 V and a pressure of 60 mmHg. TiO2 photocatalysts with metal films layered above TiO2 were also prepared using the same procedure.

2.4 Photocatalyst characterization

The crystallographic properties of the prepared Ag/TiO2 and Cu/TiO2 thin films were obtained using X-ray diffraction using a Bruker D8 Advance instrument with a Cu-Kα1 (λ − 1.54060 nm) X-ray tube and a LynxEye detector. The scanning range was from 2 theta value of 25º to 90º. The structure and morphology of the nanoparticles forming the thin films were analysed by HRSEM using an Auriga Zeiss Field Emission Scanning Electron Microscope where the SmartSem 5 software supplied with the instrument was used to capture images and AZTEC 1.2 program was used to do EDS (energy dispersive spectroscopy). The samples were sputter coated with carbon prior to HRSEM analysis. Rutherford Backscattering Spectrometry (RBS) measurements were performed with 2 MeV alpha ($4He^+$) particles using 6 MV Van de Graaff accelerator. The scattering angle was θ = 165º and the detector resolution was 20 KeV. The beam current was approximately 50 nA. The AFM analysis was performed in Nanosurf and the data was handled by the easyScan software.

2.5 Photocatalytic activity evaluation

The photocatalytic activities of the thin films were evaluated based upon the removal of methyl orange as a model pollutant. The Ag/TiO2 and Cu/TiO2 thin films on fused silica were immersed in a 10 ppm (30.6 μM) methyl orange solution. The methyl orange solution was prepared using distilled water. The solution was then irradiated with UV light of wavelength 254 nm. Aliquots were taken after every 30 min for UV−vis analysis at a wavelength of 468 nm.

4

Table 2
Sample description and codes.

Sample description	Sample Code
TiO$_2$ film with no metal film	T1
TiO$_2$ deposited on 5 nm Cu film	T5Cu
TiO$_2$ deposited on 10 nm Cu film	T10Cu
TiO$_2$ deposited on 20 nm Cu film	T20Cu
TiO$_2$ deposited on 25 nm Cu film	T25Cu
TiO$_2$ deposited on 5 nm Ag film	T5Ag
TiO$_2$ deposited on 10 nm Ag film	T10Ag
TiO$_2$ deposited on 20 nm Ag film	T20Ag
TiO$_2$ deposited on 25 nm Ag film	T25Ag
TiO$_2$ deposited on Ag (5 nm) and Cu (5 nm)	TAC
2 nm Ag film deposited on TiO$_2$ film	2AgT
5 nm Ag film deposited on TiO$_2$ film	5AgT
2 nm Cu film deposited on TiO$_2$ film	2CuT
5 nm Cu film deposited on TiO$_2$ film	5CuT

The schematic representation of the experimental set up is shown in Fig. 1. The experiments were done in a dark room to exclude ambient light. A control experiment (CE) was done with no catalyst but with UV light irradiation. The best photocatalyst in photodegrading methyl orange was also tested for its photocatalytic activity towards bisphenol A (BPA) of concentration 43.8 μM using the same experimental conditions as those used for methyl orange. The change in concentration of BPA was also determined by UV−vis analysis at a wavelength of 586 nm.

3. Results and discussion
3.1 Film deposition
The rate of deposition of the metal films was difficult to control as it was fluctuating with time hence the graphs of rate of deposition against time were plotted to see the changes in deposition during the deposition process. Although the rate of deposition varied, the resulting films were uniform. To study the effect of noble metal loading, different metal film thickness of 5 nm, 10 nm, 20 nm and 25 nm were deposited on fused silica. The graphical representation of the experimental deposition rate and change of thickness with time for Ag films is shown in Fig. 2.

The 2 nm Ag film took only a minute to deposit and fluctuations in the rate of deposition were minimal when compared to other films. As the film thickness increased, the rate of deposition became more difficult to control and the fluctuations were higher, hence the deposition rates were constantly varied (increased or reduced) by changing the current until the desired thickness was achieved.

5

3.1.1 HRSEM analysis

The HRSEM of pure uncoated fused silica (Fig. 3A) shows that the surface was smooth and uniform. A comparison of the HRSEM image of pure uncoated fused silica and MPTMS surface treated fused silica (Fig. 3B) showed that the MPTMS layer was successfully rmed on fused silica. The HRSEM images of the 10 nm monomettallic Cu and Ag metal films film (Fig. 3C & D respectively) show that the nanoparticles were uniformly distributed on the surface of fused silica support. There were significant differences in the morphology between the Cu and Ag films due to the differences in the particle size. The Ag particles were roughly spherical in shape and they did not have a uniform size but ranged from 68 to 200 nm whereas the copper nanoparticles were so small that their size could not be determined from the HRSEM images but from XRD (Fig. 6) using the Scherrer equation. The average particle size of the copper nanoparticles was found to be 6.95 nm (Table 3). The Ag film had smaller nanoparticles at the bottom than on top showing that as the thermal evaporation process continued, the size of the nanoparticles increased with an increase in film thickness due to coalescence resulting in a wide particle size distribution (polydispersed nanoparticles). The copper film did not show any variation of particle size with thickness and had a unform particle size resulting in a smooth surface. TiO_2 film deposited on fused silica was agglomerated on some sections of fused silica (Fig. 4 2E).

3.1.2 Rutherford backscattering spectrometry (RBS) measurements

RBS analysis was performed to determine the elements in fused silica and the deposited films. Fused silica in its pure form consists of only silicon and oxygen and RBS analysis of fused silica support showed that only those two elements were present and these were labelled in green (Fig. 4A). This shows that fused silica supports used in this study, were pure and had been cleaned thoroughly as no other elements were detected. The RBS analysis of 10 nm Ag coated fused silica (Fig. 4B) and 10 nm Cu coated fused silica (Fig. 4C) confirmed the presence of copper and silver in their respective films as expected. The spectra show well-defined peaks at high energies, caused by Cu and Ag and onset of scattering at lower energies due to the various constituents of the fused silica substrate. In the Ag film, very small traces of sulphur were found and in the copper films some traces of titanium were also found which may be due to handling contamination. Likewise, the peak due to titanium found in the 10 nm Cu film could be due to contamination. The detected oxygen in both the Cu and Ag films were ascribed to fused silica support.
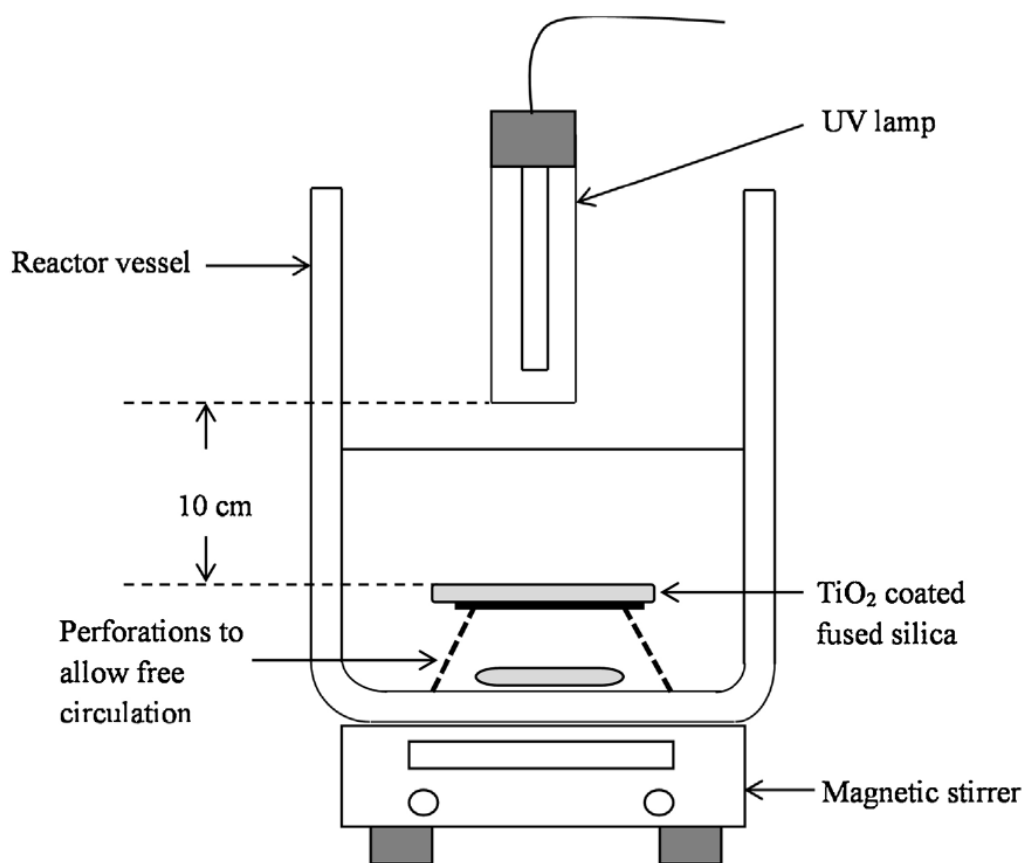
6

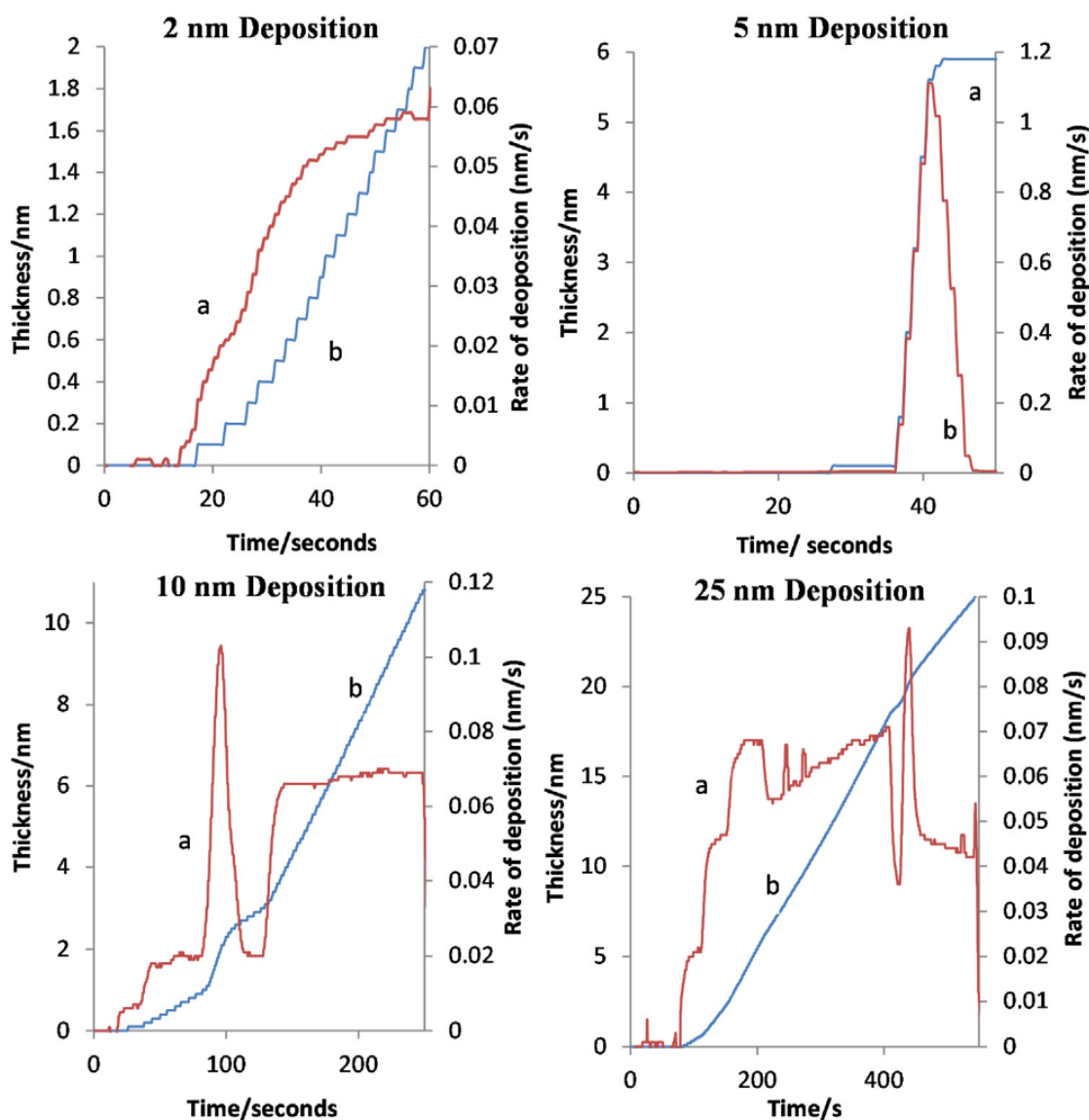**Fig. 1.** Schematic diagram showing the set-up for the photocatalytic activity experiment.

Fig. 2. Graphs of (a) rate of deposition and (b) film thickness of 2 nm, 10 nm, 20 nm, and 25 nm Ag films.

3.1.3 AFM analysis

AFM is a versatile and powerful tool for surface imaging at the nanometer to submicrometer level as it reveals surface characteristics of thin films. The three dimensional AFM surface plots for a 10 nm Cu and 10 nm Ag films and their corresponding line profiles are shown in Fig. 5. Although the nanoparticles were uniformly distributed over the MPTMS surface modified fused silica, the thin films were fairly rough. Both the 10 nm gold and silver films had a rough surface with some islands due to the coalescence of the nanoparticles during thermal deposition as the films' thickness increased. The observed islands were of different heights and shape and they were more pronounced in the Cu film. The observed surface roughness is advantageous in photocatalysis in two ways; (i) it increases the geometric surface area for adsorption of contaminants (ii) and helps to improve the adhesion of the TiO2 photocatalyst that was deposited on top of the plasmonic metal films. The reason why the

8

surfaces were rough could be that, the deposition rate was difficult to maintain and that the fused silica was etched by hydrofluoric acid before deposition.

3.1.4 XRD analysis

The XRD analysis was done on plasmonic metal films of 25 nm and pure TiO_2 (100 nm) so as to identify the peaks due to plasmonic metals before the deposition of TiO_2 and determine the peaks due to TiO_2. A thickness of 25 nm for plasmonic metals was chosen for XRD analysis so as to get clearer peaks.

In the XRD pattern of pure TiO_2 (Fig. 6), the peaks at 2u values of 27.53⁰ and 55.21⁰ indicated the presence of TiO_2 in the rutile phase while peaks at 2u values of 26.31⁰, 37.89⁰, 48.87⁰ and 64.33⁰ indicated the presence of the anatase phase showing the presence of both phases [12,13]. The peaks at 2u = 39.15⁰ , 44.60⁰ , 64.58⁰ and 77.72⁰ in the XRD pattern of the 25 nm Ag film were assigned to the diffraction from (111), (200), (220) and (311) lattice planes of pure face centred silver crystals respectively [14,15]. This also indicated that the Ag particles were crystalline in nature. No peaks were observed in the XRD pattern of MPTMS treated fused silica substrate. In the XRD pattern of 25 nm Cu film, the Bragg's reflections for the copper films were observed in the XRD pattern at 2u values of 42.61⁰, 50.68⁰ and 73.84⁰ which corresponded to (111), (200) and (220) planes of face centred cubic (fcc) structure of copper [16]. It can be seen that some traces of copper oxide were present in the copper film as evidenced by the XRD peaks at 2 theta values of 36.58⁰ and 61.52⁰. The sharp peaks in the diffraction pattern of copper indicated the presence of crystalline domains.

The diameter (D) of the copper crystalline grains attributed to nanoparticles was determined by the Debye-Scherrer equation as follows:

$$D = \frac{K\lambda}{\beta \cos \theta}$$

where K is the Scherrer constant, λ is the wavelength of light used for the diffraction, β is the "full width at half maximum" of the peaks, and θ is the Bragg diffraction angle. The calculated particle sizes of the copper nanoparticles are shown in Table 3 and the particle size ranged from 3.96 nm to 11 nm.
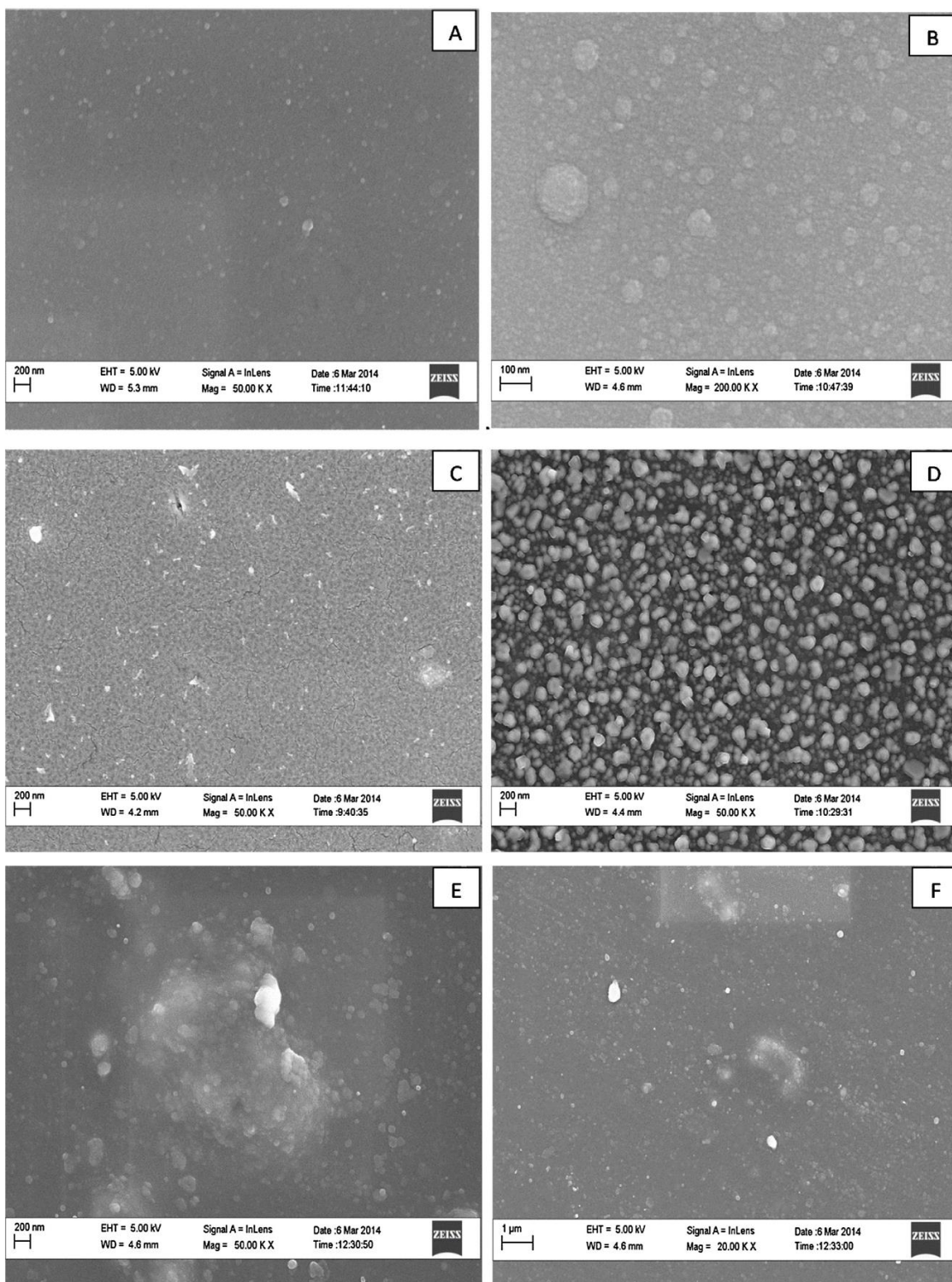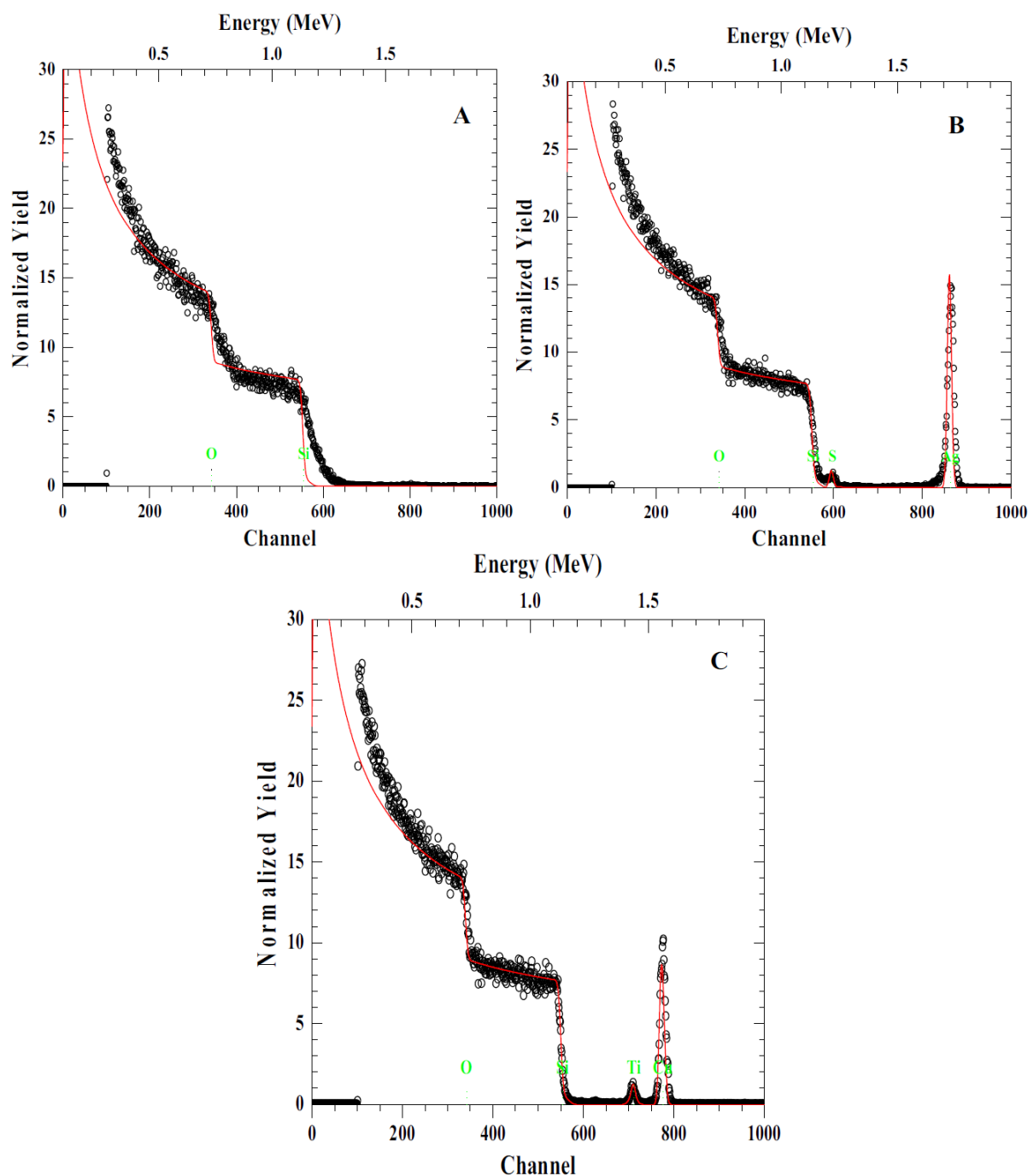
Fig. 3. HRSEM of (A) pure fused silica (50 kX), (B) MPTMS treated fused silica (200 kX), (C) copper film (50 kX), (D) 10 nm silver film (50 kX) and (E & F) TiO₂ deposited on top of plasmonic silver films at 50.00 kX and 20 kX respectively.

10

Table 3
XRD parameters and particle size of copper nanoparticles.

2 theta	Intensity (%)	FWHM	Crystal size (nm)
42.61	26.6	0.320	5.89
50.68	1.30	0.553	3.96
73.84	8.90	0.453	11.00

Fig. 4. RBS analysis of (A) uncoated fused silica, (B) 10 nm Ag coated fused silica and (C) 10 nm Cu coated fused silica.
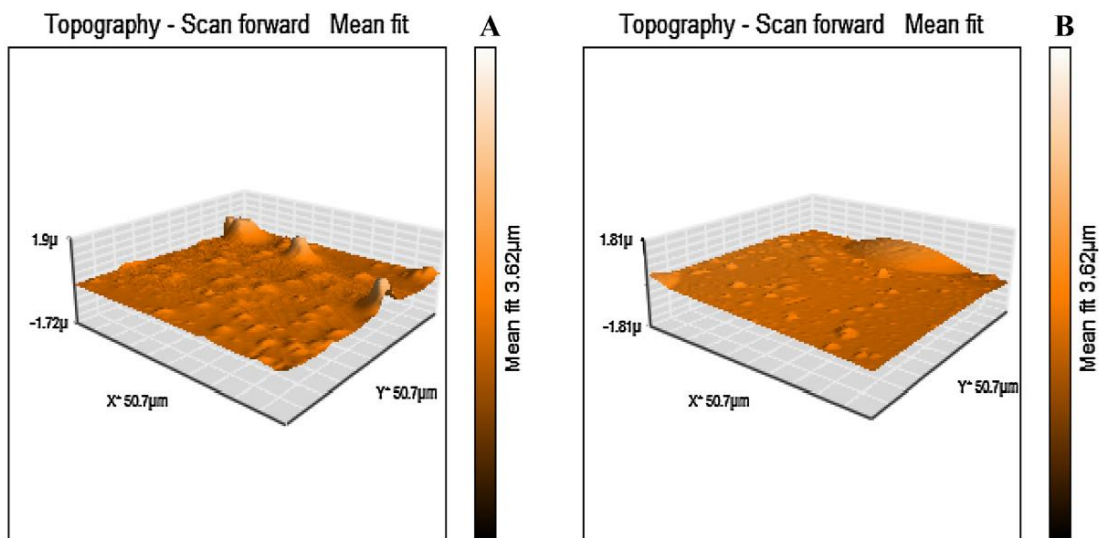
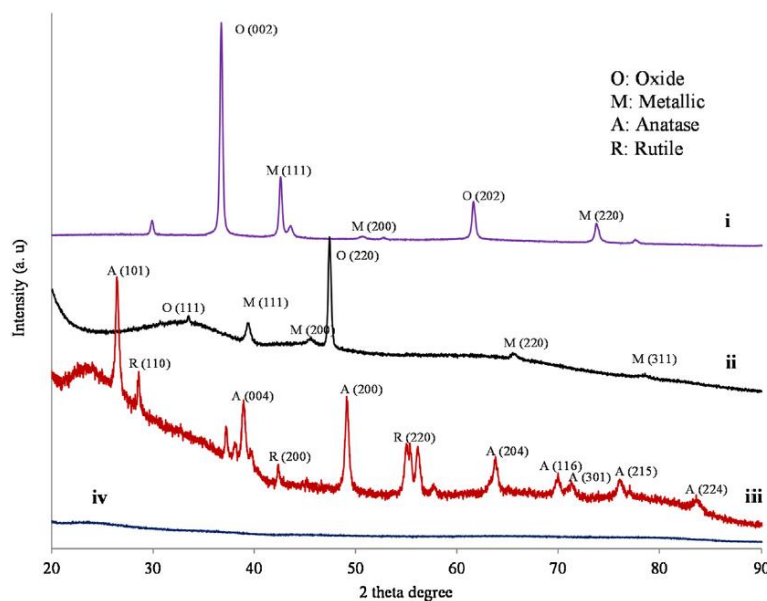**Fig. 5.** AFM topography of fused silica coated with (A) Cu film and (B) Ag film.

Fig. 6. XRD patterns (i) 25 nm copper film, (ii) 25 nm silver film, (iii) 100 nm TiO_2 film and (vi) pure fused silica.

The effect of layering of the plasmonic metals below the TiO_2 layer on the photocatalytic activity of TiO_2 was investigated using different metal film thicknesses. This was done so as to find the optimum thickness of each metal film for enhanced TiO_2 photocatalytic activity. Cu and Ag were investigated separately to find out which metal enhanced the most. The use of a bilayer system and the effect of the order of deposition were also investigated. These various experiments were conducted so as to achieve the greatest enhancement of TiO_2 photocatalytic activity.

12

3.2.1. *Effect of film thickness using silver*

Generally the effect of film thickness for the four photocatalysts (T5Ag, T10Ag, T20Ag and T25Ag) was enhanced photocatalytic activity when compared to the pure TiO_2 photocatalyst under UV light (Fig. 7) and the 20 nm Ag layer gave the highest degradation of methyl orange showing an optimum for the film thickness. The reason for the observed increase in photocatalytic activity of the metal coated TiO_2 photocatalyst is therefore ascribed to the Schottky barriers formed between the TiO_2 and the Ag nanoparticles. These barriers may facilitate the transfer of electrons from TiO_2 nanoparticles with high Fermi level to silver nanoparticles which have a low Fermi level, resulting in reduced electron-hole recombination rates. These results are similar to those reported in literature on the production of hydrogen in a photocatalytic process using Ag/TiO_2, Au/TiO_2, and Pt/TiO_2 [17]. In that study, it was found out that hydrogen production was enhanced by the metals due to the formation of Schottky barriers which promoted photogenerated electron transfer.
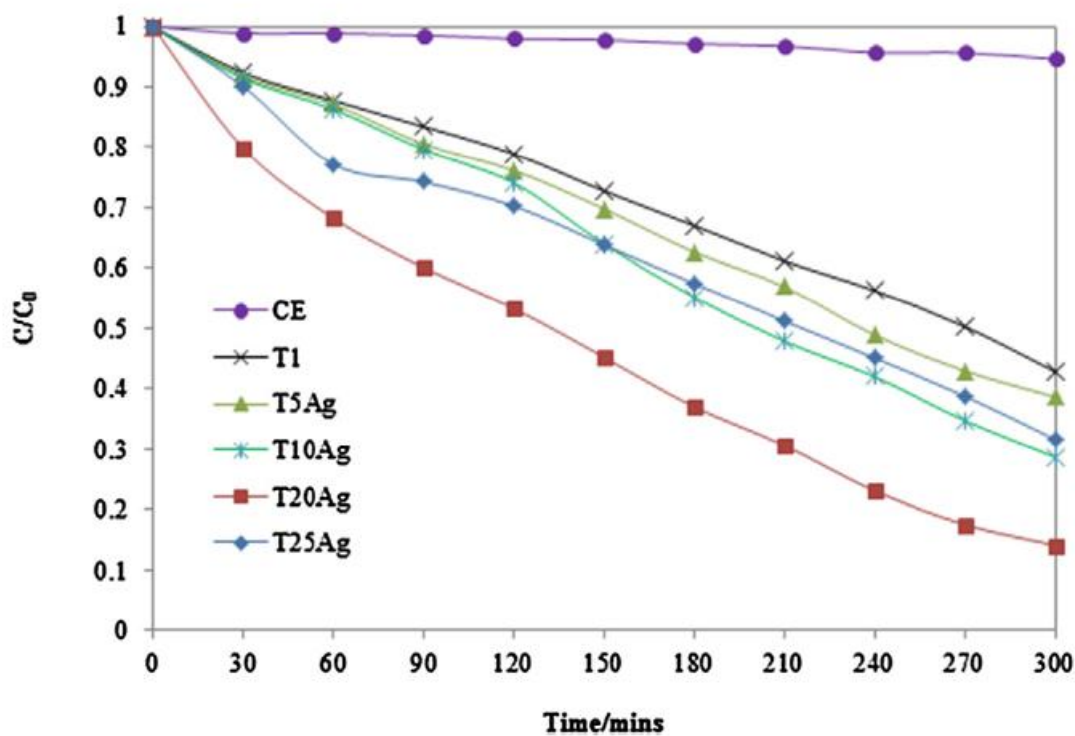

Fig. 7. Photodegradation profiles of methyl orange (10 ppm) using fused silica coated TiO_2 photocatalyst deposited on Ag films of different thicknesses (5, 10, 20 and 25 nm), T1 (pure TiO_2) and CE (control experiment) under UV light at 25 °C and pH 7. (For interpretation of the references to colour in this figure legend, the reader is referred to the web version of this article.)
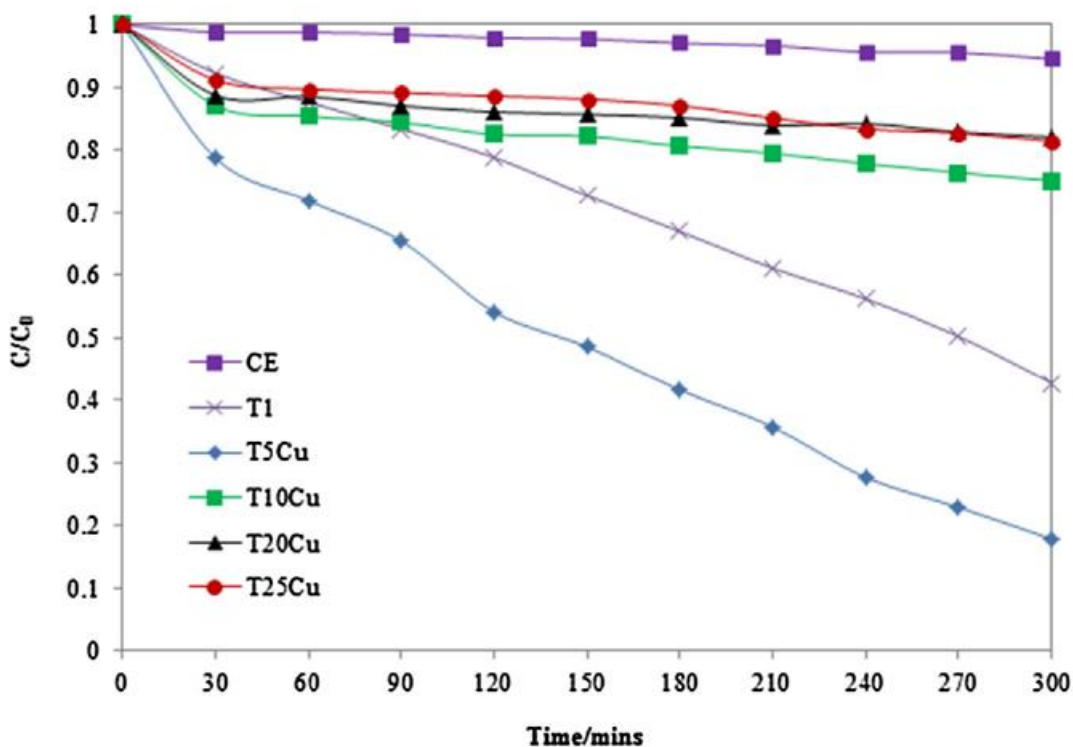
13

Fig. 8. Photodegradation curves of methyl orange (10 ppm) using fused silica coated TiO₂ photocatalyst film deposited on top of Cu films of different thicknesses (5, 10, 20 and 25 nm) under UV light at 25 °C and pH 7.

In another study, the transformation of para-aminothiophenol to p,p'-dimercaptoazobenzene occurred on grapheme due to Ag nanoparticles and the chemical reaction was controlled by the localised surface plasmon [18].

There was a gradual increase in the photodegradation of methyl orange as the Ag metal film thickness was increased from 5 nm to 20 nm. Further increases in film thickness to 25 nm caused a decrease in TiO₂ photocatalytic activity by 16.89% implying that 20 nm was the optimum layer thickness of Ag. The results are summarized in Table 3 and the general trend for the films in enhancing TiO₂ photocatalytic activity was T20Ag > T10Ag > T25Ag > T5Ag > T1. The reason for the observed trend was that, the thicker the Ag metal film the better the displacement of the electrons to lower layers of the metal film preventing recombination thus the charge separation was better when compared with thin Ag metal films. This would result in the surface of TiO₂ being enriched with holes which can directly degrade methyl orange and oxidize water to produce hydroxyl radicals that degrade organics effectively.

3.2.2 Effect of film thickness using copper
Fig. 8 shows the photodegradation curves of methyl orange using 100 nm TiO₂ photocatalyst film deposited on top of Cu films of different thicknesses

14

(T5Cu, T10Cu, T20Cu and T25Cu) on fused silica support compared to TiO_2 itself and CE which was the control experiment).

A higher photodegradation rate of methyl orange was observed in the first 30 min when compared to later times and this was characteristic for all copper films underneath the TiO_2 photocatalyst. The highest photocatalytic activity was achieved when TiO_2 was deposited on a 5 nm Cu film which was the thinnest film and any further increase in the Cu metal film thickness above 5 nm had a detrimental effect on the photocatalytic activity. The photocatalytic activities of all the photocatalysts with Cu film thicknesses above 5 nm were below the photocatalytic activity of T1 (bare TiO_2).

The relatively higher performance with a 5 nm Cu film under UV light when compared to pure TiO_2 is due to the fact that, copper nanoparticles (CuNPs) trap electrons from TiO_2 thereby reducing electron-hole recombination rates and also the resulting increase in electron density in CuNPs gives rise to a shift in plasmon since the surface plasmon resonance band intensity and wavelength depends the electron charge density [19]. The reason for the observed trend T5Cu > T1 > T10Cu > T25Cu > T20Cu could also be due to the presence of Cu^{2+} ions in solution due to leaching. These Cu^{2+} ions have been found to retard the photocatalytic activity of TiO_2 due to, (i) the short circuiting reaction which causes electron- hole recombination and (ii) the deposition of Cu metal which causes a reduction in the light reaching TiO_2 [20]. However, there is controversy in literature about the effect of Cu^{2+} on the photo-degradation rate. Some authors mention an increase in photo-degradation rate until an optimum concentration [21] while others mention a detrimental effect [22].

3.2.3 Comparison of the effect of Cu and Ag on TiO₂ photocatalytic activity

This section summarizes and compares the effect of using different plasmonic metals on the photocatalytic activity of TiO_2 towards methyl orange solution. The control experiment used pure TiO_2 photocatalyst film on fused silica, the fixed parameter was the metal thickness, and the variable was the type of the plasmonic metal used. The percentage photodegradation of methyl orange at 25 ^{O} C and pH 7 under UV light using TiO_2 photocatalyst on top of different plasmonic metal layers are shown in Table 4.

It can be seen from Table 3 that for a 5 nm metal film, the highest enhancement of 24.86% was achieved by copper whereas silver showed

only 4.17%. The 10 nm, 20 nm and 25 nm metal films of copper had a negative impact on the photocatalytic activity of TiO_2. They inactivated the photocatalyst and the resulting photo- degradation of the methyl orange under UV light was reduced by 32.36%, 39.32% and 38.68% respectively when compared to the pure TiO_2 photocatalyst with no metal film underneath. When TiO_2 was deposited on top of the metal film, there were two advantages that favoured photocatalysis and these were (i) reduced leaching of metal nanoparticles, and (ii) prevention of metal oxidation as TiO_2 acts as a protective layer for the metal nanoparticles. Unlike copper, all the film thicknesses of silver used in this study improved the photocatalytic activity of TiO_2 towards methyl orange when compared to the pure TiO_2 photocatalyst. The optimum film thickness for Ag was 20 nm which gave the best overall TiO_2 photocatalytic activity enhancement, whereas for copper it was the 5 nm layer.

3.2.4 Effect of order of deposition
The evaluation of the effect of order of deposition of metal films relative to the TiO_2 photocatalyst film was done to determine the best metal film position (top or bottom) for the enhancement of photocatalytic activity of TiO_2 towards methyl orange. A thin film of noble metal was deposited either on top of the fused silica supported TiO_2 photocatalyst or underneath the TiO_2 photocatalyst, as reported previously. The control was pure TiO_2, the variable was the position of the plasmonic metal relative to TiO_2 photocatalyst film andhe fixed parameters were the type of plasmonic metal and film thickness. Each plasmonic metal was evaluated separately.

Table 4
Percentage degradation of methyl orange at 25 °C and pH 7 under UV light using TiO_2 photocatalyst on different metal films of different thicknesses.

Photocatalyst	% of Methyl orange photodegraded after 300 min		% Increase relative to pure TiO_2 photocatalyst	
	Ag	Cu	Ag	Cu
TiO_2 on 0 nm	57.16	57.16	–	–
TiO_2 on 5 nm	61.33	**82.04**	+4.17	+24.86
TiO_2 on 10 nm	71.32	24.80	+14.16	−32.36
TiO_2 on 20 nm	**85.27**	17.84	+28.11	−39.32
TiO_2 on 25 nm	68.38	18.48	+11.22	−38.68

The choice of using very thin films of 2 nm and 5 nm on top of TiO_2 was based on trying to minimize leaching of the noble metal nanoparticles (MNP) into the water as they would be in direct contact with water.

When a 2 nm or 5 nm film of a noble metal element Ag was deposited either on top or underneath TiO_2 photocatalyst film, there was better photocatalytic activity in both cases when compared to pure TiO_2. A 2 nm Ag film deposited on top of TiO_2 photocatalyst showed 85.85% degradation of methyl orange after 300 min (5 h) but when the same Ag film thickness was deposited underneath the TiO_2 photocatalyst film, there was a decrease

16

in photocatalytic activity to 68.38% for the same degradation reaction time. The same trend was also observed when the order of deposition was changed for the 5 nm Ag film but the change (6.12%) was insignificant as shown in Table 4. The reasons for the better performance of Ag in enhancing TiO_2 photocatalytic activity when deposited on top for both the 2 nm and 5 nm films rather than when it is deposited underneath TiO_2 film could be: (i) Ag absorbs in the UV region hence it created localised surface plasmon resonance (LSPR) which boosted excitation of electrons in TiO_2 [23] and (ii) the oxidation of silver into silver oxide (silver slightly oxidizes to AgO) [24]. The resulting oxide could participate in the photodegradation of methyl orange resulting in high efficiency of the photocatalytic system. The formation of the oxide is supported by the appearance of a minor peak at 2θ value of 33.4° which was assigned to the silver oxide (Ag_2O) in the XRD spectrum of the silver film (Fig. 6) implying that some part of the deposited Ag was oxidised but not to a great extent as can be observed from the intensity of the peak which was relatively lower.

When copper film (2 nm) was used, it also followed the same trend as silver. It increased TiO_2 photocatalytic activity more when the film was deposited on top of TiO_2 (65.50%) than when it was deposited underneath the TiO_2 photocatalyst (60.85%). The reason for this could be that, Cu can be easily oxidised when exposed to air forming its oxides which can participate in the photodegradation process. The Cu_2O and CuO are p-type semiconductors with narrow band gaps of 1.2 eV and 2.2 eV respectively [25]. The formation of these oxides is evidenced by the appearance of three peaks arising from the oxides in the XRD spectrum (Fig. 6).

When the 5 nm copper film was used, the trend was opposite to that of the 5 nm silver. The copper enhanced photocatalytic activity of TiO_2 better when the 5 nm film was deposited underneath TiO_2 film (82.04%) than when deposited on top of TiO_2 photocatalyst film (68.90%). The reason for this observation could be that, there was a reduction in surface area of TiO_2 when the 5 nm copper metal film was on top and some TiO_2 active sites were covered. This could have resulted in reduced contact between the pollutant and TiO_2 photocatalyst surface during photodegradation. The effect of reduction in surface area in the case of silver was counteracted by the fact that, the experiments were done using UV light and Ag absorbs in the UV region hence it created localised surface plasmon resonance (LSPR) which boosted excitation of electrons in TiO_2 unlike copper which absorbs in the visible region. The results of the above findings on the effect of the order of deposition for all the two plasmonic elements under study are summarized in Table 5.

Generally all the 2 nm and 5 nm plasmonic metal decorated TiO_2 photocatalyst films showed higher photocatalytic activity than the pure TiO_2 film due to the creation of the Schottky barriers between the metal nanoparticles and the TiO_2 photocatalyst. This facilitated the movement of electrons resulting in reduced electron-hole recombination rates. The experiments were all performed under UV light irradiation thus the effects observed could not be ascribed to band gap engineering. The proposed mechanism of enhancement of the TiO_2 photocatalyst by the plasmonic metal is shown in Fig. 9.

3.2.5. Effect of using a bilayer metal film

The use of a bilayer metal film was explored so as to find out whether two metals would be better than the monolayer of the metal film in enhancing TiO_2 photocatalytic activity. Instead of using one noble metal film, two different noble metal films (Cu & Ag) were deposited, layer by layer. In the bimetallic layers, each metal was 5 nm thick to give a total thickness of 10 nm for both metals underneath the TiO_2 photocatalyst layer. This was done so that the observed effect would relate to the different combinations and not the metal film thickness. The use of the bilayer metal films was compared to the monolayer of the same thickness. In this experiment the Ag film was in contact with the TiO_2 film and the Cu film was in contact with fused silica support. Table 6 presents data on percentage degradation of methyl orange using TiO_2 photocatalyst on 10 nm metal films of either Cu or Ag compared to mixed Ag/Cu bilayers.

Table 5
Percentage degradation of methyl orange under UV light using TiO_2/plasmonic MNP films with different orders of deposition.

Plasmonic element & thickness	% Degradation of MeO under UV light		% Change when metal film was on top instead of underneath TiO_2
	Metal film on top of TiO_2	Metal film underneath TiO_2	
2 nm Ag film	**85.85**	68.38	+17.47
5 nm Ag film	67.45	61.33	+6.12
2 nm Cu film	65.50	60.85	+4.65
5 nm Cu film	68.90	82.04	−13.14

Table 6
Percentage degradation of methyl orange using TiO_2 photocatalyst on 10 nm metal films (monometallic and bimetallic layers) under UV light.

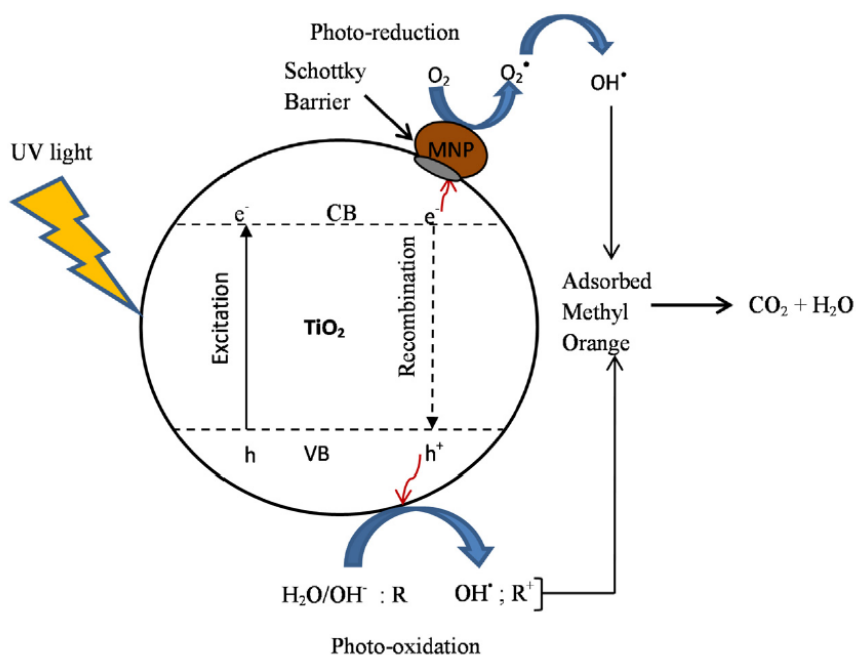| Photocatalyst	Metal thickness	% Photodegradation after 300 min
T1	0 nm	57.16
T10Cu	10 nm	24.80
T10Ag	10 nm	71.32
TAC	Ag (5 nm)/Cu (5 nm)	74.36

18

Fig. 9. Schematic representation of the proposed mechanism of activation of TiO2, electron trapping by metal nanoparticles (MNP) and photodegradation of MeO under UV light.

The photocatalytic activity of T10Cu and T10Ag towards methyl orange was 24.80% and 71.31% respectively but when TiO_2 was deposited on a bilayer of Cu and Ag (TAC) of the same thickness, the photodegradation increased to 74.36% which was slightly higher than TiO_2 on monometallic films. This showed that when these two metal layers were combined, they worked synergistically and performed better than a single metal layer since the metals could augment one another. When two metals whose work functions are different are brought into contact, charge transfer occurs whereby electrons flow from the metal with higher Fermi energy to that with lower Fermi energy. In this case the order of the work functions was φ Cu $^>$ φ Ag $^>$, hence electrons were flowing to the metal from the semiconductor on contact. In a bilayer system, there are more than two contacts (TiO_2/metal, metal/metal and metal/fused silica support) resulting in more than two Schottky barriers being formed which promote efficient electron transfer from the photocatalyst. This could have caused the observed enhanced photocatalytic activity of TiO_2 by bilayer metal film.
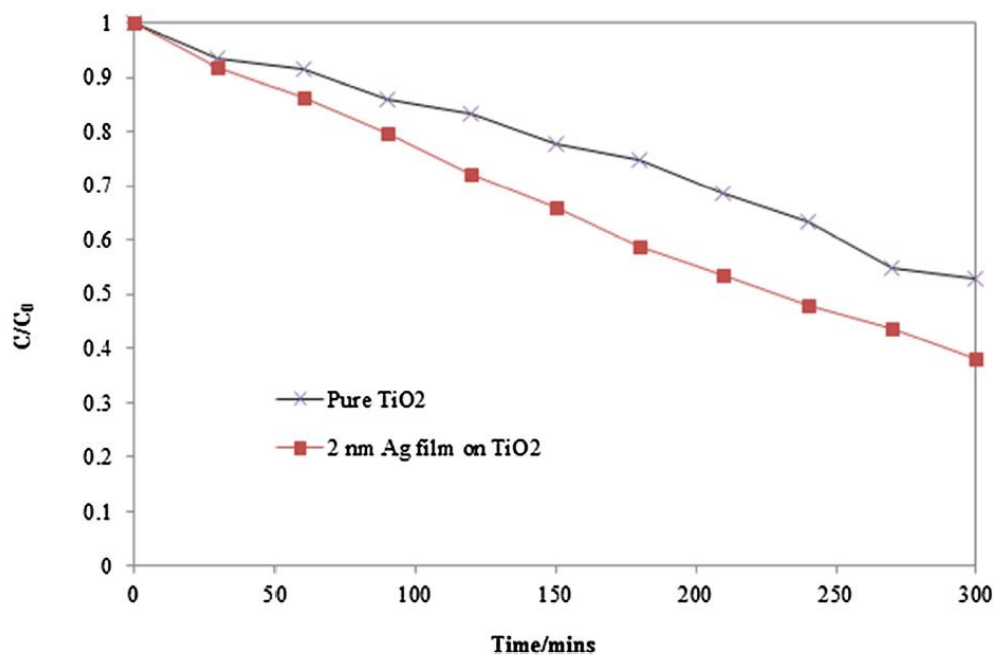
Fig. 10. Photodegradation profiles of 100 mL of 10 ppm BPA solution under UV light at 25 °C and pH 7 using pure TiO_2 and TiO_2 with 2 nm Ag on top.

3.2.6. BPA photodegradation

The most active plasmonic metal decorated TiO_2 photocatalyst (2 nm Ag on TiO_2) in the photodegradation of methyl orange was also tested for its photocatalytic activity towards BPA which is an endocrine disruptor. The photocatalyst degraded 61.86% of BPA after 300 min (Fig. 10) which was 23.99% lower when compared to methyl orange photodegradation (ca. 85.85%). The same trend was also observed using pure TiO_2 photocatalyst which degraded 47.10% of BPA which was 10.06% lower than that of methyl orange (ca. 57.16%). These results show that BPA is more difficult to degrade than methyl orange under the same conditions.

There are three possible reasons why these two contaminants were not degraded to the same extent even when the same mass and volume were used and these are: (i) methyl orange has a higher molar absorption coefficient than BPA hence its rate of degradation will be higher, (ii) methyl orange could have been more adsorbed on the photocatalyst than BPA. It is known that a contaminant needs to be in contact with the catalyst for it to be degraded hence if it is adsorbed more readily then its degradation is promoted. It has been reported that organic substrates with electron withdrawing nature strongly adhere to the photocatalyst and are more susceptible to direct oxidation than those with electron donating groups [26]. In this study, methyl orange had more electron withdrawing groups than BPA, (iii) the azo bonds in the azo compounds are active and are easily degraded. It has also been reported that azo bonds

20

are the most active in azo-dye molecules hence would be susceptible to attack by positive holes and hydroxyl radicals [27].

4 Conclusions

Copper and silver films were successfully deposited on MPTMS treated fused silica using a thermal evaporation technique and TiO$_2$ films were deposited using the sputter coating technique. HRSEM showed that the plasmonic metal nanoparticles were uniformly distributed on the fused silica substrates. The highest photo-degradation of methyl orange (85.85%) after 5 h was achieved by the TiO$_2$ photocatalyst film with 2 nm Ag film on top. Ag nanoparticles were found to perform better in enhancing TiO$_2$ photocatalytic activity when they were deposited on top of the TiO$_2$ photocatalyst rather than underneath whereas copper performed better when it was deposited underneath TiO$_2$ film than on top. Overall, silver films were more suitable than copper in enhancing TiO$_2$ photocatalytic activity which is ascribed to the localised surface plasmon resonance effect of Ag. The use of bimetallic layers increased the photodegradation of methyl orange from 24.8% for T10Cu and 71.32% for T10Ag to 74.36% for the bimetallic film of the same thickness as a result of the synergistic effect of the two metals.

http://repository.uwc.ac.za

References

[1] U.G. Akpan, B.H. Hameed, Parameters affecting the photocatalytic degradation of dyes using TiO_2-based photocatalysts: a review, J. Hazard. Mater. 170 (2009) 520–529.

[2] W.Z. Tang, H. An, UV/TiO_2 photocatalytic oxidation of commercial dyes in aqueous solutions, Chemosphere 31 (1995) 4158–4170.

[3] U.I. Gaya, A.H. Abdullah, Heterogeneous photocatalytic degradation of organic contaminants over titanium dioxide: a review of fundamentals progress and problems, J. Photochem. Photobiol. C: Photochem. Rev. 9 (2008) 1–12.

[4] A. Alinsafi, F. Evenou, E.M. Abdulkarim, M.N. Pons, O. Zahraa, A. Benhammou,
4.2 Yaacoubi, A. Nejmeddine, Treatment of textile industry wastewater by supported photocatalysis, Dyes Pigm. 74 (2007) 439–445.

[5] Z. Zainal, L.K. Hui, M.Z. Hussein, Y.H. Taufiq-Yap, A.H. Abdullah, I. Ramli, Removal of dyes using immobilized titanium dioxide illuminated by fluorescent lamps, J. Hazard. Mater. 125 (2005) 113–120.

[6] T. Ochiai, K. Nakata, T. Murakami, A. Fujishima, Y. Yao, D.A. Tryk, Y. Kubota, Development of solar-driven electrochemical and photocatalytic water treatment system using a boron-doped diamond electrode and TiO_2 photocatalyst, Water Res. 44 (2010) 904–910.

[7] J. Xu, X. Xiao, A.L. Stepanov, F. Ren, W. Wu, G. Cai, S. Zhang, Z. Dai, F. Mei, C. Jiang, Efficiency enhancements in Ag nanoparticles-SiO_2-TiO_2 sandwiched structure via plasmonic effect-enhanced light capturing, Nanoscale Res. Lett. 8 (2013) 73.

[8] E. Liu, L. Kang, Y. Yang, T. Sun, X. Hu, C. Zhu, H. Liu, Q. Wang, X. Li, J. Fan, Plasmonic Ag deposited TiO_2 nano-sheet film for enhanced photocatalytic hydrogen production by water splitting, Nanotechnology 25 (2014) 1–10.

[9] J. Xu, Z. Wang, W. Li, X. Zhang, D. He, X. Xiao, Ag nanoparticles located on ThreeDimensional pine tree-like hierarchical TiO_2 nanotube array films as high efficiency plasmonic photocatalysts, Nanoscale Res. Lett. 12 (2017) 1–9.

[10] X. Zhang, B. Wang, X. Wang, X. Xiao, Z. Dai, W. Wu, C. Jiang, Preparation of M@ $BiFeO_3$ nanocomposites (M = Ag, Au) bowl arrays with enhanced visible light photocatalytic activity, J. Am. Ceram. Soc. 98 (2015) 2255–2263.

[11] J. Chen, K.N. Struk, A.B. Brennan, Surface modification of silicate glass using 3- (mercaptopropyl) trimethoxysilane for ThiolEne polymerization, Langmuir 27 (2011) 13754–13761.

[12] D.D. Mulmi, D. Thapa, B. Dahal, D. Baral, P.R. Solanki, Spectroscopic studies of boron doped titanium dioxide nanoparticles, Int. J. Mater. Sci. Eng. 4 (2016) 172–178.

[13] K. Thamaphat, P. Limsuwan, B. Ngotawornchai, Phase characterization of TiO_2 powder by XRD and TEM, J. Nat. Sci. 42 (2008) 357–361.

[14] F. Liao, Z.F. Wang, X.Q. Hu, Shape controllable synthesis of dendritic silver nanostructures at room temperature, Colloid J. 73 (2011) 504–508.

[15] B. Liu, M. Wang, Electrodeposition of dendritic silver nanostructures and their application as hydrogen peroxide sensor, Int. J. Electrochem. Sci. 8 (2013) 8572–8578.

[16] M. Salavati-Niasari, F. Davar, Synthesis of copper and copper (I) oxide nanoparticles by thermal decomposition of a new precursor, Mater. Lett. 63 (2009) 441–443.

[17] G.L. Chiarello, M.H. Aguirre, E. Selli, Hydrogen production by photocatalytic steam reforming of methanol on noble metal-modified TiO_2, J. Catal. 273 (2010) 182–190.

[18] Z. Dai, X. Xiao, W. Wu, Y. Zhang, L. Liao, S. Guo, J. Ying, C. Shan, M. Sun, C. Jiang, Plasmon-driven reaction controlled by the number of graphene layers and localized surface plasmon distribution during optical excitation, Light: Sci. Appl. 4 (2015) 342.

[19] X. Huang, M.A. El-Sayed, Gold nanoparticles: optical properties and implementations in cancer diagnosis and photothermal therapy, J. Adv. Res. 1 (2010) 13–28.

[20] M.R. Dhananjeyan, V. Kandavelu, R. Renganathan, An investigation of the effects of Cu^{2+} and heat treatment on TiO_2 photo-oxidation of certain pyrimidines, J. Mol. Catal. A: Chem. 158 (1997) 577–582.

[21] V. Brezova, A. Blaskova, E. Borsova, M. Ceppan, R. Fiala, The influence of dissolved metal ions on the photocatalytic degradation of phenol in aqueous TiO_2 suspensions, J. Mol. Catal. A: Chem. 98 (1995) 109–116.

[22] T.Y. Wei, Y.Y. Yang, C.C. Wan, Kinetics of photo-catalytic oxidation of phenol on TiO_2 surface, J. Photochem. Photobiol. A. 69 (1992) 241–249.

[23] M.K. Hedayati, F. Faupel, M. Elbahri, Review of plasmonic nanocomposite metamaterial absorber, Materials 7 (2014) 1221–1248.

[24] T.M.D. Dang, T.T.T. Le, E. Fribourg-Blanc, M.C. Dang, Synthesis and optical properties of copper nanoparticles prepared by a chemical reduction method, Adv. Nat. Sci.: Nanosci. Nanotechnol. 2 (2011) 1–6.

[25] J.M. Zheng, G. Song, C.W. Kim, Y.S. Kang, One-step transformation of Cu to Cu_2O in alkaline solution, RSC Adv. 4 (2014) 18616.

[26] D.S. Bhatkhnade, S.P. Kamble, S.B. Sawant, V.G. Pangarkar, Photocatalytic and photochemical degradation of nitrobenzene using artificial ultraviolet light, Chem. Eng. J. 102 (2004) 283–290.

[27] E.M. Saggioro, A.S. Oliveira, T. Pavesi, C.G. Maia, L.F.V. Ferreira, J.C. Moreira, Use of titanium dioxide photocatalysis on the remediation of

model textile wastewaters containing Azo dyes, Molecules 16 (2011) 10370–10386.